

## Raman Lidar MERGE Value-Added Product

RK Newsom  
C Sivaraman

J Goldsmith

April 2017

## **DISCLAIMER**

This report was prepared as an account of work sponsored by the U.S. Government. Neither the United States nor any agency thereof, nor any of their employees, makes any warranty, express or implied, or assumes any legal liability or responsibility for the accuracy, completeness, or usefulness of any information, apparatus, product, or process disclosed, or represents that its use would not infringe privately owned rights. Reference herein to any specific commercial product, process, or service by trade name, trademark, manufacturer, or otherwise, does not necessarily constitute or imply its endorsement, recommendation, or favoring by the U.S. Government or any agency thereof. The views and opinions of authors expressed herein do not necessarily state or reflect those of the U.S. Government or any agency thereof.

## **Raman Lidar MERGE Value-Added Product**

RK Newsom, Pacific Northwest National Laboratory (PNNL)  
Principal Investigator

J Goldsmith, PNNL  
C Sivaraman, PNNL  
Co-Investigators

April 2017

Work supported by the U.S. Department of Energy,  
Office of Science, Office of Biological and Environmental Research

## Acronyms and Abbreviations

AGL	above ground level
ARM	Atmospheric Radiation Measurement
ASCII	American Standard Code for Information Interchange
CBH	cloud base height
DMF	Data Management Facility
DOE	U.S. Department of Energy
Hz	hertz
km	kilometer
m	meter
mJ	millijoule
mrاد	milliradian
MHz	megahertz
nm	nanometer
ns	nanosecond
NFOV	narrow-field-of-view zenith radiometer
netcdf	Network Common Data Form
PMT	photomultiplier tube
PNNL	Pacific Northwest National Laboratory
RL	Raman lidar
s	second
UTC	Coordinated Universal Time
VAP	value-added product or process
WFOV	wide-field-of-view zenith radiometer

## Contents

Acronyms and Abbreviations .....	iii
1.0 Introduction .....	1
2.0 Input Data .....	3
3.0 Algorithm and Methodology .....	4
3.1 Conversion to Photon Counting Rate and Analog Voltage.....	4
3.2 Analog Delay .....	5
3.3 Pulse Pile-up Correction.....	6
3.4 Cloud Base Height .....	7
3.5 Dark Current.....	8
3.6 Gluing.....	9
3.7 Error Estimates.....	13
4.0 Output Data .....	13
5.0 Summary.....	15
6.0 References .....	15

## Figures

1 Layout of the ARM Raman lidar optics.....	1
2 Raw data flow. Profiles of photon counting and analog data from each of the detection channels are stored in separate ASCII files.....	2
3 Raman lidar data flow within the DMF.....	2
4 a) Examples of analog voltage (red) and photon counting rate (blue) profiles, and b) photon counting rate versus analog voltage for the same data in panel a).....	6
5 Effects of the pulse pile-up correction on the photon counting rate data.....	7
6 CBH detection process.....	8
7 Corrected photon counting rate versus analog voltage for the narrow-field-of-view N <sub>2</sub> (387 nm) channel on 16 March 2017 for the ARM Southern Great Plains (SGP) Raman lidar.....	9
8 Uncorrected (green), corrected (blue), and merged (red) photon counting rate profiles for the NFOV nitrogen channel at ~6 UTC on 16 March 2017 for the SGP Raman lidar.....	11
9 (Top) Time-height cross-section of the merged photon counting rates for the narrow-field-of-view elastic (355 nm) channel; (Middle) cloud base height; (Bottom) “merge flag” indicating which samples are corrected photon counting rates (blue), which samples are virtual photon counting rates (red), and which samples are saturated or clipped (white).....	12
10 Time series of (a) the analog offset, $A_o$ , and (b) the scale factor, $s$ , for the narrow-field-of-view N <sub>2</sub> channel for the SGP Raman lidar.....	13

## Tables

1	The MERGE VAP configuration files and their information content.....	3
2	Variable names from the raw RL datastream that serve as inputs to the MERGE VAP.....	3
3	Variable names from the RLPROFMERGE2NEWS datastream.....	14

## 1.0 Introduction

The U.S. Department of Energy (DOE) Atmospheric Radiation Measurement (ARM) Climate Research Facility Raman lidars (RLs) are semi-autonomous, land-based, laser remote sensing systems that provide height- and time-resolved measurements of water vapor mixing ratio, temperature, aerosol backscatter, extinction, and linear depolarization ratio from about 200 m to greater than 10 km AGL. These systems transmit at a wavelength of 355 nm with 300 mJ, ~5 ns pulses, and a pulse repetition frequency of 30 Hz. The receiver incorporates nine detection channels, including two water vapor channels at 408 nm, two nitrogen channels at 387 nm, three elastic channels, and two rotational Raman channels for temperature profiling at 354 and 353 nm.

Figure 1 illustrates the layout of the ARM RL receiver system. Backscattered light from the atmosphere enters the telescope and is directed into the receiver system (i.e., aft optics). This signal is then split between a narrow-field-of-view radiometer (NFOV) path (blue) and a wide-field-of-view zenith radiometer (WFOV) path (red). The WFOV (2 mrad) path contains three channels (water vapor, nitrogen, and unpolarized elastic), and the NFOV (0.3 mrad) path contains six channels (water vapor, nitrogen, parallel and perpendicular elastic, and two rotational Raman). All nine detection channels use Electron Tubes 9954B photomultiplier tubes (PMTs). The signals from each of the nine PMTs are acquired using transient data recorders from Licel GbR (Berlin, Germany).

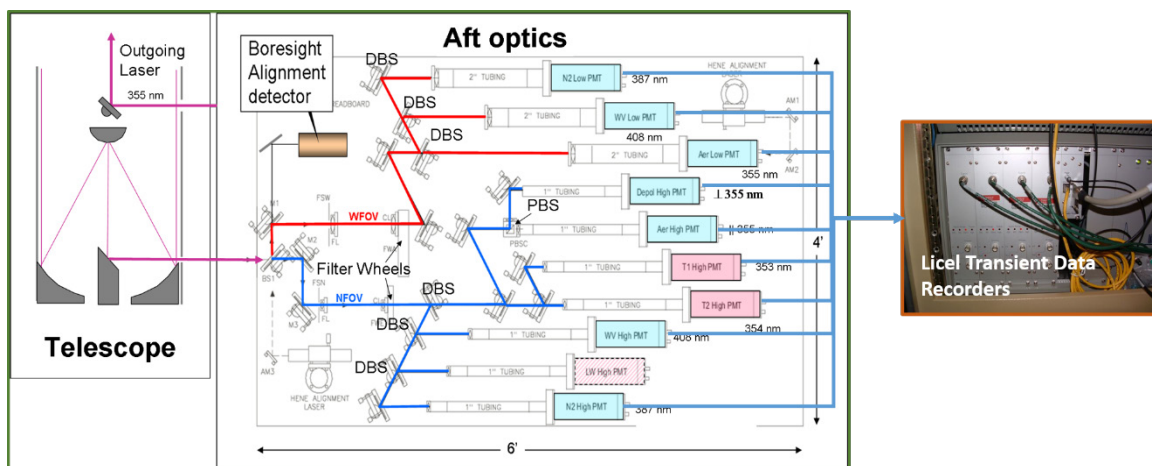


**Figure 1.** Layout of the ARM Raman lidar optics. The atmospheric return enters the aft optics where it is split between a narrow-field-of-view path (RED) and a wide-field-of-view path (BLUE). The signals from each of the PMTs are routed into separate Licel data recorders.

The Licel data recorders provide simultaneous measurements of both analog photomultiplier current and photon counts at height resolution of 7.5 m and a time resolution of 10 s. The analog signal provides good linearity in the strong signal regime, but poor sensitivity at low signal levels. Conversely, the photo counting signal provides good sensitivity in the weak signal regime, but is strongly nonlinear at higher signal levels. The advantage in recording both signals is that they can be combined (or merged) into a single signal with improved dynamic range. The process of combining the analog and photon counting data has become known as “gluing” (Whiteman *et al.*, 2006).

The gluing process for the ARM RLs is accomplished by the so-called MERGE value-added process (VAP). The MERGE VAP then provides the input data for the “higher-level” RL VAPs (e.g., water vapor mixing ratio, temperature, aerosol backscatter, etc.). This report describes the gluing algorithm used by the MERGE VAP, as well as the input and output data.

Figure 2 illustrates the data flow from the lidar to the ARM Data Management Facility (DMF). The digital signals from the Licel recorders are stored locally on the instrument computer as ASCII files. Each ASCII file contains photon counts and analog voltages from each of the nine detection channels for a single 10 s profile. The ASCII files are collected by the DMF and converted to twice-daily netCDF files. Each profile contains 4,000 range bins for the NFOV and 1,500 range bins for the WFOV channels.

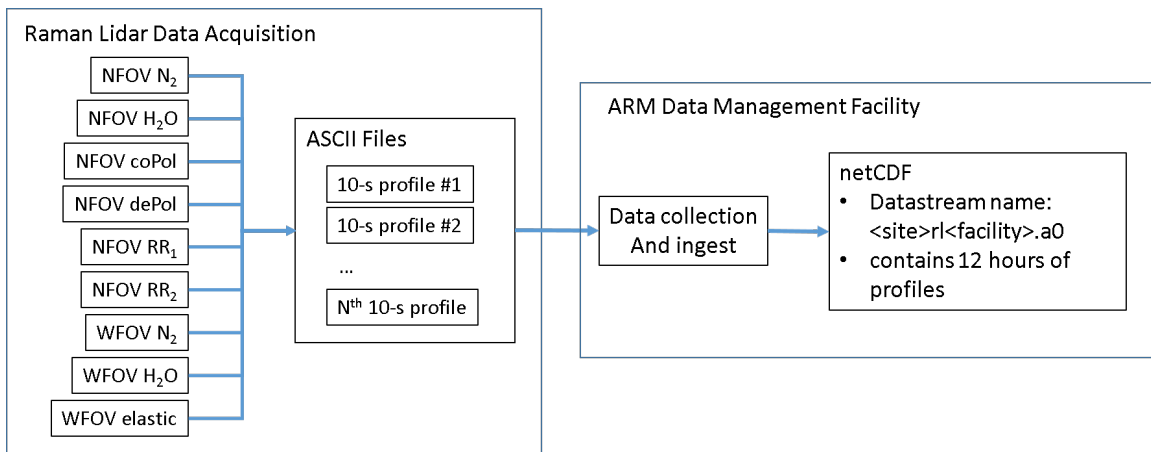


**Figure 2.** Raw data flow. Profiles of photon counting and analog data from each of the detection channels are stored in separate ASCII files. These ASCII files are collected by the DMF and accumulated into twice-daily netCDF files.

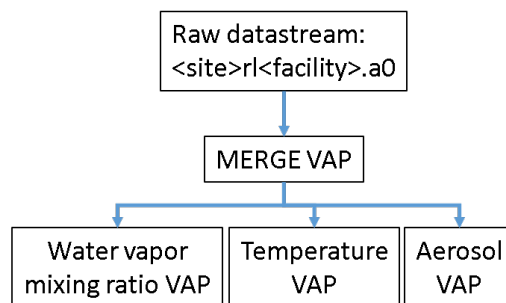


**Figure 3.** Raman lidar data flow within the DMF. The MERGE VAP functions as an intermediary between the raw datastream and the higher-level RL VAPs.

## 2.0 Input Data

The input for the MERGE VAP comes from the raw Raman lidar datastream, <site>rl<facility>.a0, and three configuration files. The configuration files contain system constants and other parameters that are used in the gluing process. Table 1 lists the configuration files and the information they contain. Additionally, Table 2 lists the variables from the <site>rl<facility>.a0 datastream that are used by the MERGE VAP.

**Table 1.** The MERGE VAP configuration files and their information content.

Configuration File Name	Information Content
rlprof_merge_glue.conf	$\tau, s, A_o, C_{min}, C_{max}$ for each detection channel.
rlprof_merge_system.conf	$n_o, n_{offset}, \Delta r, A_{max}, \beta$
rlprof_merge_temp.conf	Location descriptions of the various thermocouples used to monitor the internal temperature of the lidar.

**Table 2.** Variable names from the raw RL datastream that serve as inputs to the MERGE VAP. The wildcards (\*) refer to “water”, “nitrogen”, “t1”, “t2”, “depolarization”, and “elastic” for the NFOV (high) channels, and to “water”, “nitrogen”, and “elastic” for the WFOV (low) channels. Note that the number of shots summed is the same for all detection channels; thus, the “shot\_summed\_\*\_high” and “shot\_summed\_\*\_low” variables contain redundant data.

Variable Name	Dimensions	Description
base_time	Scalar	Start time in seconds since 0 UTC 1 January 1970
time_offset	Time	Elapsed time since start time (s)
pulse_energy	Time	Laser pulse energy (mJ)
acquisition_time	Time	Pulse integration time
Filter	Time	Filter wheel position, 0=beam blocked, 1 or 2 =beam NOT blocked
Rh	Time	Relative humidity inside the lidar container
temp1, temp2, temp2, temp3, temp4	Time	Internal laser system temperatures
temp5, temp6, s1, s2, s3	Time	Internal lidar temperatures
s4, s5, s6, s7, s8, n2_cloud_check_value	Time	Alignment system parameters
lat, lon, alt	Scalars	Latitude, longitude, and altitude of the lidar
shots_summed_*_high	Time	Number of laser pulses accumulated
*_counts_high	Time, height	Accumulated photon counts for the NFOV * channel
*_analog_high	Time, height	Accumulated analog signal for the NFOV * channel
shots_summed_*_low	Time	Number of laser pulses accumulated
*_counts_low	Time, height	Accumulated photon counts for the WFOV * channel
*_analog_low	Time, height	Accumulated analog signal for the WFOV * channel

## 3.0 Algorithm and Methodology

Newsom *et al.* (2009) describes the MERGE VAP. Here we provide further data-processing details.

### 3.1 Conversion to Photon Counting Rate and Analog Voltage

For a given detection channel the MERGE VAP first reads in the analog voltage and photon counting data from the raw netCDF files, i.e., the raw RL datastream. The MERGE VAP processes data from one 24-hour period at a time. The analog voltage and photon counting data from the raw data files are two-dimensional arrays that depend on time and height. Each profile is obtained by accumulating returns over a 10 s period. Thus, the number of beams in one 24-hour period is typically slightly less than  $24 \times 3600 / 10 = 8640$ .

We denote the raw photon counting signal by

$$N_{ij}^{photon} = N^{photon}(t_i, z_j), \quad (1)$$

and the raw analog signal by

$$A_{ij}^{raw} = A^{raw}(t_i, z_j), \quad (2)$$

where  $t_i$  is the time of the  $i^{th}$  profile, and  $z_j$  is the height of the  $j^{th}$  range gate. The height of the  $j^{th}$  range gate is determined from

$$z_j = \Delta r(j - n_o), \quad (3)$$

where  $n_o$  is the so-called ‘‘ground bin’’, and  $\Delta r$  is the range gate size, as defined in the ‘‘rlprof\_merge\_system.conf’’ configuration file (see Table 1). Currently, the range gate size for all the ARM Raman lidars is 7.5 m. The ground bin defines the range bin corresponding to the ground altitude. We note that data acquisition begins several microseconds before the laser pulse is triggered. Thus, the system records the ambient background for  $j < n_o$  or  $z_j < 0$ .

The first step in the MERGE VAP is to convert photon counts to photon counting rates in units of MHz, and the raw analog values to millivolts. The uncorrected photon counting rate is given by

$$C_{ij}^{raw} = \frac{c}{2\Delta r} \frac{N_{ij}^{photon}}{N_i^{shots}} \quad (4)$$

where  $c$  is the speed of light ( $3 \times 10^8 \text{ ms}^{-1}$ ), and  $N_i^{shots}$  is the number of laser shots accumulated during the pulse integration period. The analog voltage is computed from

$$A_{ij} = g \frac{A_{ij}^{raw}}{N_i^{shots}} \quad (5)$$

where  $g$  is the analog gain and is given by

$$g = A_{\max} / 2^{\beta-1} \quad (6)$$

where  $A_{\max}$  is the gain setting on the Licel unit, and  $\beta=12$  is resolution of the digitizer in bits. These parameters are defined in the “rlprof\_merge\_system.conf” configuration file (see Table 1). For the ARM Raman lidars we use  $A_{\max} = 20\text{mV}$ .

### 3.2 Analog Delay

The analog signal has an inherent delay relative to the photon counting data. Thus, a correction is applied whereby the analog profile is shifted by a few range bins in order to optimize agreement with the photon counting profile. This correction takes the following form:

$$A_{ij} \rightarrow A(t_i, z_j - n_{\text{offset}} \Delta r) \quad (7)$$

where  $n_{\text{offset}}$  is the range bin offset of the analog signal relative to the photon counting signal, and is defined in the “rlprof\_merge\_system.conf” configuration file (see Table 1). The range bin offset is a fixed property of the Licel data recorders and may be different for each Licel unit. This parameter is determined through offline analysis and typically ranges between 3 and 10.

Examples of typical analog voltage and photo counting rate profiles are provided in Fig 4a. For  $z < 0$  the system records the ambient light background. We note also that the analog signal has an inherent electronic background level that is superimposed on the ambient signal. At  $z=0$  the pulse leaves the lidar, and both the analog voltage and photon counting rate signals register a sharp spike, which we refer to as the ground spike.

Figure 4b shows the photon counting rate as a function of the analog voltage for the same data shown in Fig 4a. In this example the analog range bin offset was determined to be 10, and the ground bin was determined as 329. The distinct curve in Fig 4b is due to the pulse pile-up effect in the photon counting rate data.

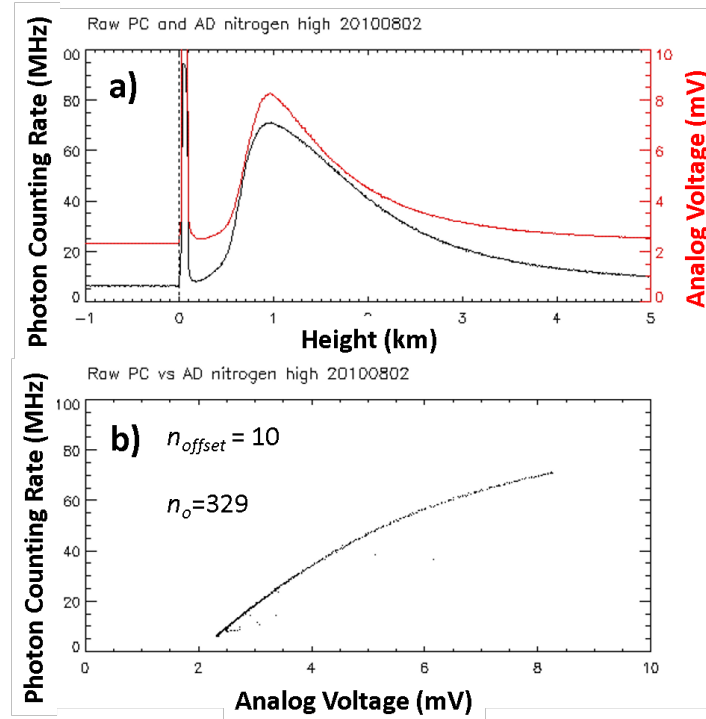


**Figure 4.** a) Examples of analog voltage (red) and photon counting rate (blue) profiles, and b) photon counting rate versus analog voltage for the same data in panel a).

### 3.3 Pulse Pile-up Correction

A pulse pile-up correction (also known as dead-time correction) is applied to the photon counting rate data. This correction takes the following form (Whiteman et al., 2006):

$$C_{ij} = \frac{C_{ij}^{raw}}{1 - \tau C_{ij}^{raw}} \quad (8)$$

where

$C_{ij}^{raw}$  = Uncorrected photon counting rate

$\tau$  = Response time, also known as “dead-time coefficient”

The response time,  $\tau$ , is a property of the photomultiplier tube (PMT) and detection electronics, and is therefore fixed for a given detection channel. This parameter typically ranges between roughly 3 and 8 ns. Figure 5 illustrates the effect that this correction has on the photon counting rate data.

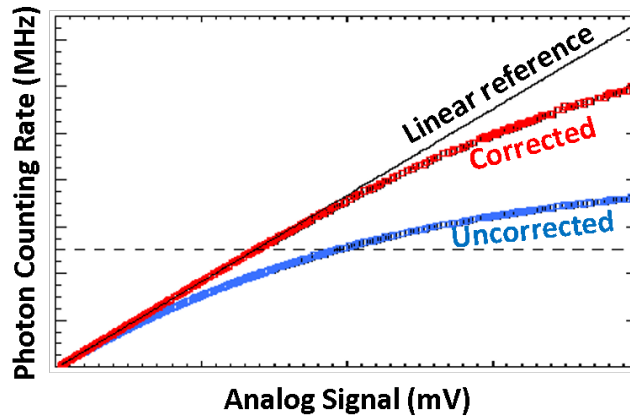


**Figure 5.** Effects of the pulse pile-up correction on the photon counting rate data. In this example, the blue (red) curve is the uncorrected (corrected) photon counting rate and the black line is a linear reference.

Response times for each detection channel are determined through offline analysis of several months of data, as described by Newsom *et al.* (2009). The response times for each detection channel are stored in the “rlprof\_merge\_glue.conf” configuration file, which is used by the MERGE VAP.

### 3.4 Cloud Base Height

It is necessary to filter out measurements effected by clouds before estimating the glue coefficients. Thus, prior to estimating the glue coefficients, the MERGE attempts to identify the heights of cloud bases by locating prominent spikes in the profiles of the analog voltage for the NFOV copolarization, NFOV depolarization, and the WFOV elastic channels.

The cloud base height (CBH) algorithm uses a method based on the first derivative of the range-corrected analog voltage profile, as illustrated in Fig 6. When a cloud is present in the profile, the first derivative, which is computed using a simple central-difference approximation, shows a strong positive peak immediately below and a strong negative peak immediately above the cloud base. We require the magnitude of these peaks to exceed 0.1 mV km, and the separation between the peaks to be between 2 and 15 range bins. If these conditions are met, then the CBH algorithm locates the maximum in the range-corrected analog voltage between these two extrema. The height of this maximum then determines the CBH. This process is then repeated for all 10 sec profiles acquired during a given 24-hour period. Additional checks are applied to minimize false detections by rejecting temporally isolated CBH estimates. This is done by computing the absolute difference in CBH between a given profile and the CBH values from profiles immediately before and after in time. If both differences exceed 1 km, then that CBH value is rejected.

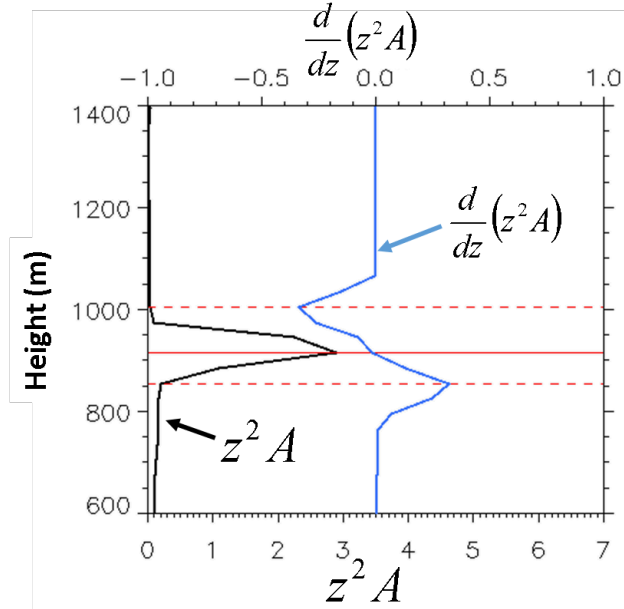


**Figure 6.** CBH detection process. The black profile represents the range-corrected analog voltage profile, and the blue curve represents the first derivative of the range-corrected analog voltage. The dashed red line highlights the locations of the minimum and maximum of the first derivative, and the solid red curve highlights the location of the maximum of the range-corrected analog voltage profile.

The CBH detection algorithm described above is applied to the NFOV copolarization, NFOV depolarization, and the WFOV elastic channels. A final “consensus” CBH value is obtained by taking the lowest of the three estimates in a given profile.

### 3.5 Dark Current

The MERGE VAP produces estimates of the “dark current” for each detection channel. The “dark current” in this case is the photon counting rate in the absence of any ambient light. It is useful for characterizing the inherent noise limit of the PMTs.

The ARM Raman lidars perform periodic “background” measurements by blocking the light entering the WFOV and NFOV paths in the aft optics. This is accomplished by using filter wheels in the WFOV and NFOV light paths. Several times a day the filter wheels rotate an opaque filter into the light path for several minutes. This results in what we refer to as “mode 0” data. These “mode 0” data are then used to compute the dark current.

The dark current is computed by accumulating the photon counts from all “mode 0” profiles acquired during a given 24-hour period, and dividing by the total acquisition time, i.e.:

$$\text{Dark current} = \frac{c}{2\Delta r} \sum_{ij} N_{ij}^{\text{photon}} / N_i^{\text{shots}}, \quad i \in \text{mode0} \quad (9)$$

where the summation is performed over all range bins,  $j$ , and overall mode0 profiles,  $i$ .

### 3.6 Gluing

The pulse pile-up correction (equation 8) helps to extend the linear range of the photon counting rate data, as illustrated in Figure 5. With the correction, the relationship between  $C_{ij}$  and  $A_{ij}$  is approximately linear for  $C_{ij} < 15$  MHz. In this linear range we define the so-called “virtual” count rate as

$$C_{ij}^{virtual} = s(A_{ij} - A_o), \quad (10)$$

where  $A_o$  is the analog background or offset, and  $s$  is the scale factor. We refer to  $A_o$  and  $s$  as “glue” coefficients.

For a given detection channel, the MERGE VAP uses linear regression between the corrected photon counting rates,  $C_{ij}$ , and the analog voltages,  $A_{ij}$ , to establish the analog offset,  $A_o$ , and scale factor,  $s$ . The regression is performed using only (non-mode-zero) data for which

$$C_{min} < C_{ij} < C_{max} \quad (11)$$

and

$$z_j < CBH_i,$$

where  $C_{min}$  and  $C_{max}$  are prescribed parameters that determine the lower and upper limit of the fit range, respectively. These parameters, which are defined in the “rlprof\_merge\_glue.conf” configuration file (see Table 1), are set to  $C_{min} = 1$  MHz and  $C_{max} = 15$  MHz.

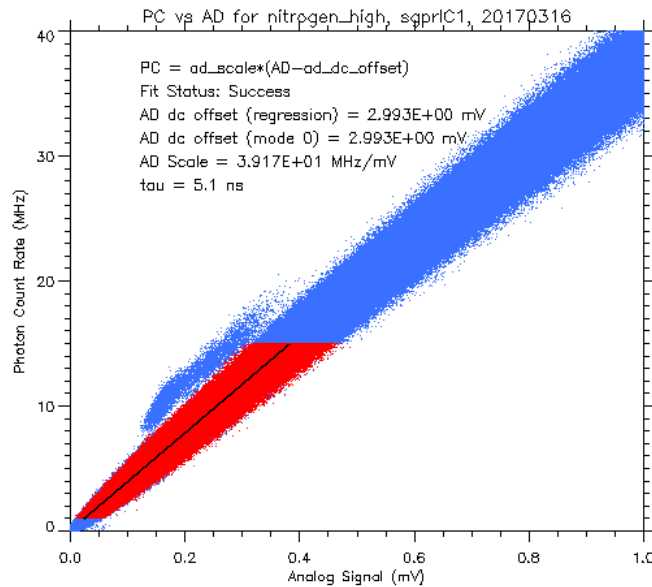


**Figure 7.** Corrected photon counting rate versus analog voltage for the narrow-field-of-view N2 (387 nm) channel on 16 March 2017 for the ARM Southern Great Plains (SGP) Raman lidar. The

red points indicates those sample that were used in the linear regression. The solid black line is the result of the linear regression.

Figure 7 shows a plot of the photon counting rates versus analog voltages for the narrow-field-of-view N<sub>2</sub> channel on 16 March 2017 from the Raman lidar at the Southern Great Plains site. The result of the linear regression is shown by the black line in Figure 7. We note that all of the measurements for a given day are used in the determination of the glue coefficients,  $A_0$  and  $s$ . The alternative is to compute time-dependent glue coefficients by performing a linear regression on each 10 s profile, but we found this approach produced poorer results in the water vapor mixing ratio (Newsom *et al.*, 2009).

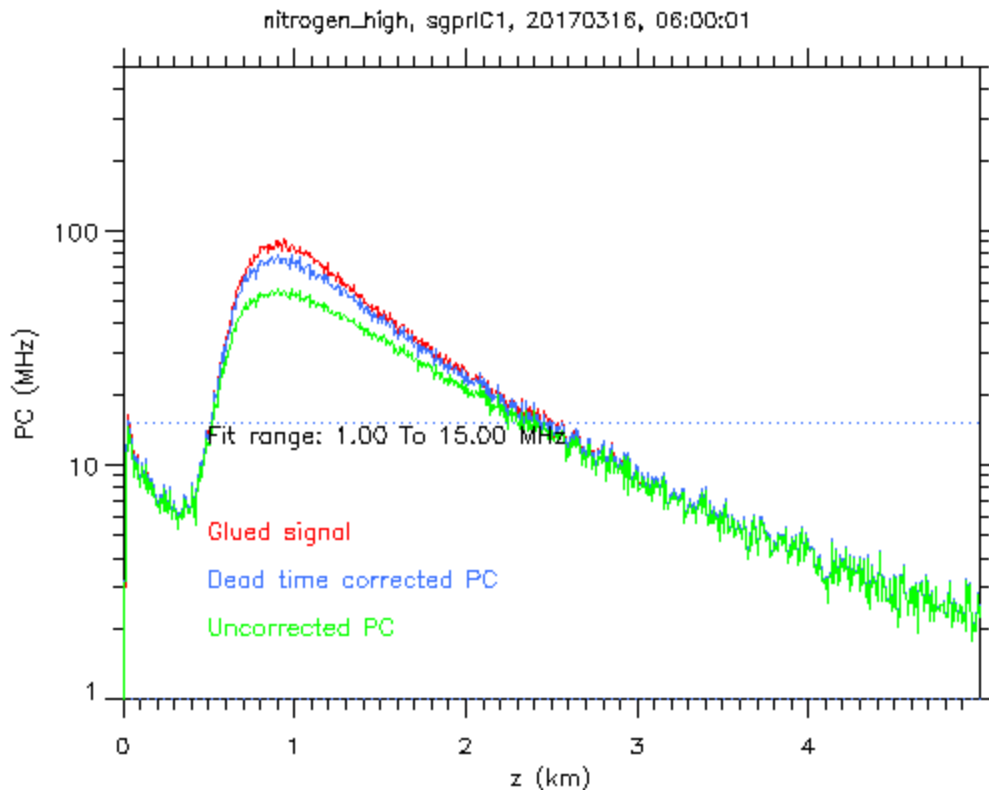
The linear regression is performed by first averaging the analog data in discrete photon counting rate bins, ranging from  $C_{min}$  to  $C_{max}$  with a bin size of 0.2 MHz. Within each bin the mean and standard deviation of the analog data is computed. The linear regression treats the analog signal as the dependent variable. Thus, the regression is performed by doing a linear least-squares fit to the bin-averaged analog data as a function of the bin-average photon counting rate data using the standard deviation of the bin-averaged analog signal as the measurement error. The linear regression is deemed successful if the fit residual (root-mean-squared difference between the fit and the bin-averaged analog data) is less than 0.01 mV, and the Pearson correlation coefficient is greater than 0.95. In that case the fit status is set to 1. If the fit residual exceeds 0.01 mV, or the correlation is below 0.95, then default glue coefficients from the “rlprof\_merge\_glue.conf” configuration file are used, and the fit status is set to 0.

Once the glue coefficients have been determined (for a given day and detection channel), the merged profiles are obtained by combining  $C_{virtual}$  and  $C$  such that

$$C_{ij}^{merge} = \begin{cases} C_{ij} & \text{for } C_{ij} < C_{max} \\ C_{ij}^{virtual} & \text{for } C_{ij} \geq C_{max} \end{cases} . \quad (12)$$

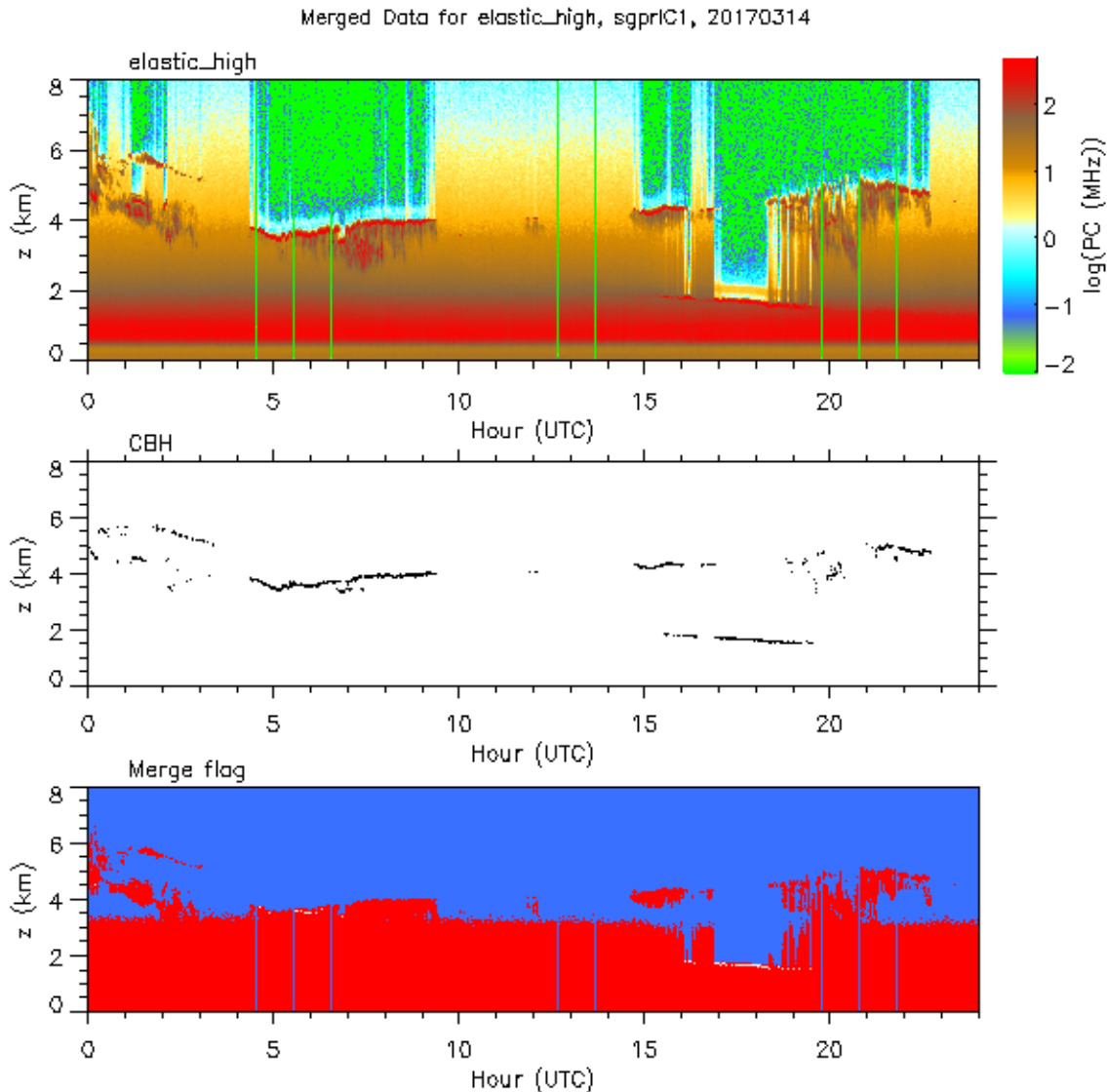
Thus, the merged profile contains the corrected photon counting rate data for  $C_{ij} < C_{max}$ , and the extrapolated virtual photon counting rate data above  $C_{max}$ .

Figure 8 shows an example of a merged profile for the narrow-field-of-view N<sub>2</sub> channel at about 6 UTC on 16 March 2017 at the Southern Great Plains site. The green curve shows the uncorrected photon counting rate data,  $C_{raw}$ , the blue curve shows corrected photon counting rate data,  $C$ , and the red curve shows the merged profile,  $C_{merge}$ . This figure shows, at least qualitatively, that the virtual counting data (red) merges seamless with the corrected photon counting rates (blue) near the transition at  $C_{max} = 15$  MHz. It also illustrates the residual nonlinearity in the “corrected” photon counting rate data above 15 MHz. By slicing in the virtual photon counting rates above 15 MHz, the merged profile exhibits improved linearity.



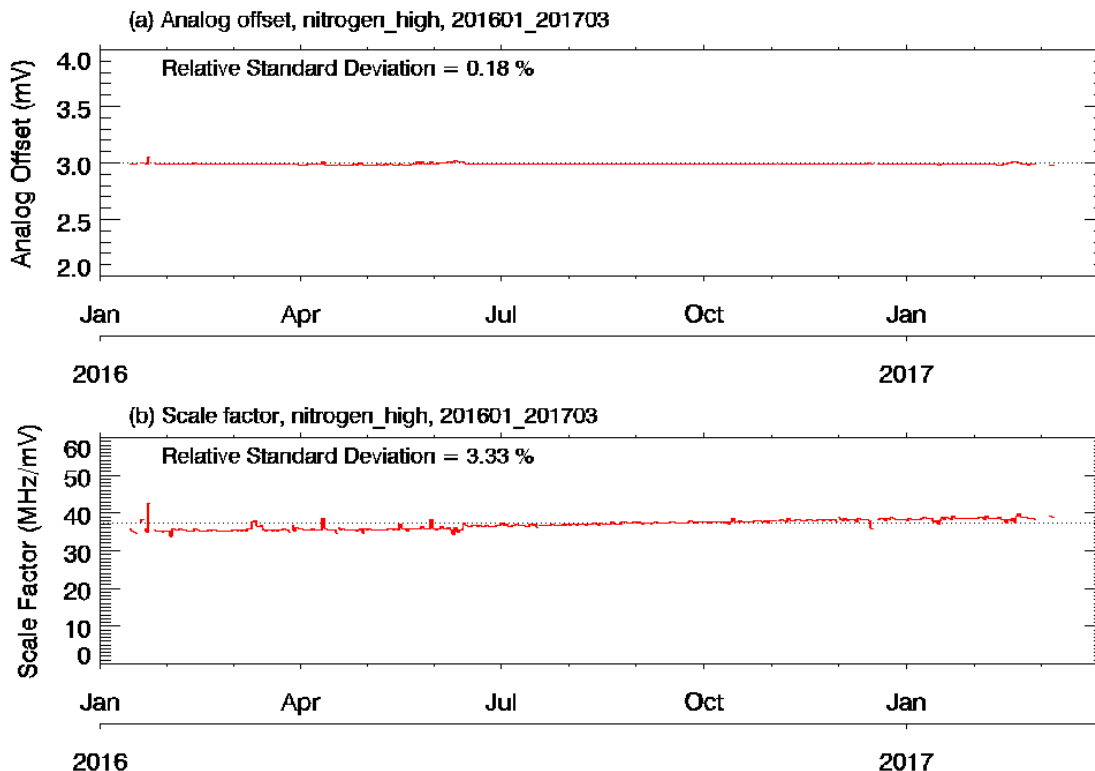
**Figure 8.** Uncorrected (green), corrected (blue), and merged (red) photon counting rate profiles for the NFOV nitrogen channel at ~6 UTC on 16 March 2017 for the SGP Raman lidar.

Figure 9a shows a time-height cross-section of the merged  $N_2$  photon counting rate data for 16 March 2017. Figure 9b shows the cloud base height estimates, and Figure 9c shows the so-called “merge flag.” The merge flag indicates which samples in Figure 9a were obtained from the corrected photon counting rates (blue) and which samples were obtained from the extrapolated virtual photon counting rates (red). Additionally, the white areas in Fig 9c indicate saturated (i.e., clipped) signals.



**Figure 9.** (Top) Time-height cross-section of the merged photon counting rates for the narrow-field-of-view elastic (355 nm) channel; (Middle) cloud base height; (Bottom) “merge flag” indicating which samples are corrected photon counting rates (blue), which samples are virtual photon counting rates (red), and which samples are saturated or clipped (white). This example was taken from the SGP RL on 14 March 2017.

Figure 10 shows time-series of the glue coefficient for the NFOV N<sub>2</sub> channel (also known as the nitrogen low channel) in the SGP Raman lidar for the period from about 1 January 2016 to about 1 March 2017. The figure shows that glue coefficients exhibit a fair degree of stability over both short- and long-term periods. For the NFOV N<sub>2</sub> channel, the analog offset,  $A_o$ , shows a relative standard deviation of 0.18% and the scale factor,  $s$ , shows a relative standard deviation of 3.3%. The analog offset shows no significant long-term variation, whereas the scale factor shows a small change over the period shown.



**Figure 10.** Time series of (a) the analog offset,  $A_o$ , and (b) the scale factor,  $s$ , for the narrow-field-of-view  $N_2$  channel for the SGP Raman lidar. The plots cover the period from about 1 January 2016 to about 1 March 2017.

### 3.7 Error Estimates

Estimates of the random uncertainty in the photon counting rate data are not explicitly provided in the output of the MERGE VAP. However, uncertainty estimates can easily be computed.

The photon counting data obey Poisson statistics. Thus, the uncertainty is given by the square root of the photon counts. Since the MERGE output is given in photon counting rates, one must first convert to counts, and then take the square-root. That result can then be converted back to a counting rate.

Mathematically, this process can be expressed in the following way:

$$\delta C_{ij} = \frac{c}{2\Delta r N_i^{shots}} \sqrt{\frac{2\Delta r}{c} C_{ij} N_i^{shots}} = \sqrt{\frac{c C_{ij}}{2\Delta r N_i^{shots}}} \quad (13)$$

## 4.0 Output Data

The output variables for the rlprofmerge2news datastream are listed in Table 3.

**Table 3.** Variable names from the RLPROFMERGE2NEWS datastream. The wildcards (\*) refer to “water”, “nitrogen”, “t1”, “t2”, “depolarization”, and “elastic” for the NFOV (high) channels, and “water”, “nitrogen”, and “elastic” for the WFOV (low) channels.

Variable Name	Dimensions	Description
base_time	Scalar	Start time in seconds since 0 UTC 1 January 1970
time_offset	Vector	Elapsed time since start time (s)
pulse_energy	Vector	Laser pulse energy (mJ)
acquisition_time	Vector	Pulse integration time
Filter	Vector	Mode, 0=beam blocked, 1 or 2=beam NOT blocked
Height_high	Vector	NFOV height array
Height_low	Vector	WFOV height array
Shots_summed	Vector	Number of laser pulses accumulated
Cbh	Vector	Cloud base height
Rh	Vector	Relative humidity inside the lidar container
temp1, temp2, temp2, temp3, temp4	Vector	Internal laser system temperatures
temp5, temp6, temp7, temp8, temp9	Vector	Internal lidar temperatures
X_mirror, y_mirror, X_display, y_display, snr_display, n2_cloud	Vector	Alignment system parameters
lat, lon, alt	Scalars	Latitude, longitude and altitude of the lidar
*_counts_high	Time, height	Accumulated photon counts for the NFOV * channel
*_counts_high_merge_flag	Time, height	Flag indicating (0) photon counting data, (1) virtual photon counting data, or (2) clipped signal for the NFOV * channel
*_counts_high_dc_offset	Time	$A_o$ for the NFOV * channel
*_counts_high_scale	Time	s for the NFOV * channel
*_counts_high_tau	Scalar	$\tau$ for the NFOV * channel
*_counts_high_pcfmin	Scalar	$C_{min}$ for the NFOV * channel
*_counts_high_pcfmax	Scalar	$C_{max}$ for the NFOV * channel
*_counts_high_fit_status	Time	Flag indicating (0) failure or (1) success of the linear regression for the NFOV * channel
*_counts_high_background	Scalar	Dark current for the NFOV * channel
*_counts_high_bin_offset	Scalar	$n_{offset}$ for the NFOV * channel
*_counts_low	Time, height	Accumulated photon counts for the WFOV * channel
*_counts_low_merge_flag	Time, height	Flag indicating (0) photon counting data, (1) virtual photon counting data, or (2) clipped signal for the WFOV * channel
*_counts_low_dc_offset	Time	$A_o$ for the WFOV * channel
*_counts_low_scale	Time	s for the WFOV * channel
*_counts_low_tau	Scalar	$\tau$ for the WFOV * channel
*_counts_low_pcfmin	Scalar	$C_{min}$ for the WFOV * channel
*_counts_low_pcfmax	Scalar	$C_{max}$ for the WFOV * channel
*_counts_low_fit_status	Time	Flag indicating (0) failure or (1) success of the linear regression for the WFOV * channel
*_counts_low_background	Scalar	Dark current for the WFOV * channel
*_counts_low_bin_offset	Scalar	$n_{offset}$ for the WFOV * channel

## 5.0 Summary

This report summarizes the data-processing steps taken by the ARM Raman lidar MERGE VAP. This VAP essentially converts the raw digital photon counting and analog data from the lidar's data-acquisition system to photon counting rate profiles that can be used by the high-level Raman lidar VAPs. These higher-level VAPs include processes for computing water vapor mixing ratio, temperature, aerosol backscatter, extinction, and depolarization ratio.

## 6.0 References

Newsom, RK, DD Turner, B Mielke, MF Clayton, R Ferrare, and C Sivaraman. 2009. "Simultaneous analog and photon counting detection for Raman lidar." *Applied Optics* 48(20): 3903-3914, [doi:10.1364/AO.48.003903](https://doi.org/10.1364/AO.48.003903).

Turner, DD, RA Ferrare, LA Heilman Brasseur, WF Feltz, and TP Tooman, 2002. "Automated retrievals of water vapor and aerosol profiles from an operational Raman lidar." *Journal of Atmospheric and Oceanic Technology* 19: 37-50.

Whiteman, DN, B Demoz, P Di Girolamo, J Comer, I Veselovskii, K Evans, Z Wang, M Cadirola, K Rush, G Schwemmer, B Gentry, SH Melfi, B Mielke, D Venable, and T Van Hove. 2006. "Raman Water Vapor Lidar Measurements during the International H<sub>2</sub>O Project. I: Instrumentation and Analysis Techniques." *Journal of Atmospheric and Oceanic Technology* 23: 157-169, [doi:10.1175/JTECH1838.1](https://doi.org/10.1175/JTECH1838.1).

